RSC Advances

PAPER

View Article Online
View Journal | View Issue

Cite this: *RSC Adv.*, 2021, **11**, 9459

Thermal-stability of the enhanced piezoelectric, energy storage and electrocaloric properties of a lead-free BCZT ceramic†

Soukaina Merselmiz, *[a] Zouhair Hanani, [abf] Daoud Mezzane,[ac]
Anna G. Razumnaya,[cd] M'barek Amjoud,[a] Lahoucine Hajji,[a] Svitlana Terenchuk,[e]
Brigita Rožič, [f] Igor A. Luk'yanchuk[ce] and Zdravko Kutnjak[f]

The lead-free $Ba_{0.85}Ca_{0.15}Zr_{0.10}Ti_{0.90}O_3$ (BCZT) relaxor ferroelectric ceramic has aroused much attention due to its enhanced piezoelectric, energy storage and electrocaloric properties. In this study, the BCZT ceramic was elaborated by the solid-state reaction route, and the temperature-dependence of the structural, electrical, piezoelectric, energy storage and electrocaloric properties was investigated. X-ray diffraction analysis revealed a pure perovskite phase, and the temperature-dependence of Raman spectroscopy, dielectric and ferroelectric measurements revealed the phase transitions in the BCZT ceramic. At room temperature, the strain and the large-signal piezoelectric coefficient (d_{33}^*) reached a maximum of 0.062% and 234 pm V^{-1}, respectively. Furthermore, enhanced recovered energy density (W_{rec} = 62 mJ cm^{-3}) and high-energy storage efficiency (η) of 72.9% at 130 °C were found. The BCZT ceramic demonstrated excellent thermal stability of the energy storage variation (ESV), less than ±5.5% in the temperature range of 30–100 °C compared to other lead-free ceramics. The electrocaloric response in the BCZT ceramic was explored *via* the indirect approach by using the Maxwell relation. Significant electrocaloric temperature change (ΔT) of 0.57 K over a broad temperature span (T_{span} = 70 °C) and enhanced coefficient of performance (COP = 11) were obtained under 25 kV cm^{-1}. The obtained results make the BCZT ceramic a suitable eco-friendly material for energy storage and solid-state electrocaloric cooling devices.

Received 15th November 2020
Accepted 22nd February 2021

DOI: 10.1039/d0ra09707a

rsc.li/rsc-advances

1. Introduction

Lead-based piezoceramics such as lead zirconium titanate ($PbZr_xTi_{1-x}O_3$, PZT) systems have aroused substantial interest due to their outstanding piezoelectric, electrocaloric and energy storage performances.[1–4] However, due to the environmental and human concerns caused by their toxicity, the integration of lead-based materials in future applications will be restricted.[3,5,6] In 2009, Liu and Ren reported a $Ba_{0.85}Ca_{0.15}Zr_{0.10}Ti_{0.90}O_3$ (BCZT) material with excellent electrical and piezoelectric properties as a revolutionary discovery in the field of ferroelectrics, which can substitute the Pb-based materials.[7] The high piezoelectricity observed in BCZT was ascribed to the low energy barrier for polarisation rotation, *i.e.*, energy landscape flattening at the morphotropic phase boundary.[7–9]

The assessment of various application-relevant properties like the cost, reproducibility, electrical conductivity, and lifetime is required to transfer the lead-free piezoceramics into products.[3] More important, the thermal-stability of the electrical properties over a broad operating temperature is a crucial requirement for the actual integration of the lead-free materials.[3,10] For this purpose, BCZT ferroelectric relaxor can fulfil this necessity due to its diffuse ferroelectric transition.[11–13] Hanani *et al.*[11] reported the thermal-stability of the energy storage and electrocaloric properties of BCZT ceramic elaborated by low-temperature hydrothermal processing, and found a small energy storage variation (ESV) of 12.7% between 27 and 127 °C, alongside with enhanced recovered energy storage (W_{rec}) of 414.1 mJ cm^{-3} at 107 °C. In addition, Puli *et al.*[14] investigated the energy storage performances in $(1-x)$BZT–xBCT ($x = 0.10$, 0.15, 0.20) system and observed improved W_{rec} and high energy storage efficiency (η) of 680 mJ cm^{-3} and 72.8%, respectively, at $x = 0.15$ under 170 kV cm^{-1}. Besides, Cai *et al.*[15] studied the effect of grain size on the dielectric, ferroelectric, piezoelectric and energy storage performances, and observed that the

---

[a] *IMED-Lab, Cadi Ayyad University, Marrakesh, 40000, Morocco. E-mail: soukaina.mers@gmail.com*

[b] *ICMCB, University of Bordeaux, Pessac, 33600, France*

[c] *LPMC, University of Picardy Jules Verne, Amiens, 80039, France*

[d] *Faculty of Physics, Southern Federal University, Rostov-on-Don, 344090, Russia*

[e] *Department of Building Materials, Kyiv National University of Construction and Architecture, Kyiv, 03680, Ukraine*

[f] *Jožef Stefan Institute, Ljubljana, 1000, Slovenia*

† Electronic supplementary information (ESI) available. See DOI: 10.1039/d0ra09707a

piezoelectric coefficient (d_{33}) gradually increases with the grain size increasing, however, despite the enhanced η, low W_{rec} and modest ESV were reported.

For eco-friendly solid-state refrigeration, BCZT ceramic demonstrated enhanced electrocaloric properties.[13,16–21] Zhou *et al.*[18] investigated the electrocaloric effect (ECE) in lead-free $(1 - x)$BZT–xBCT system under a moderate electric field of 28 kV cm^{-1} and reported high ECE response of 0.56 K at $x = 0.6$. In addition, Ben Abdessalem *et al.*[22] studied the electrocaloric effect (ECE) in BCZT indirectly using Maxwell relation under 30 kV cm^{-1} and obtained $\Delta T = 0.565$ K around $T_C = 119$ °C. Besides, Hanani *et al.*[11] reported a significant electrocaloric temperature change (ΔT) of 1.479 K with remarkable refrigerant capacity (RC) of 140.33 J kg^{-1}, and a high coefficient of performance (COP = input power/output cooling power)[23] of 6.29 under 55 kV cm^{-1}.

Recently, miniaturised devices required materials with multifunctional properties, *e.g.*, piezoelectric, electrocaloric and energy storage.[24] In this study, we report, simultaneously, the thermal-stability of the piezoelectric, energy storage and electrocaloric properties of lead-free BCZT ceramic between 30 and 150 °C under 25 kV cm^{-1}. The temperature-dependence of the structural properties in BCZT ceramic are investigated by *in situ* Raman spectroscopy. The electrocaloric effect in BCZT ceramic is revealed by an indirect approach through Maxwell relation.

2. Experimental section

Lead-free $Ba_{0.85}Ca_{0.15}Zr_{0.1}Ti_{0.9}O_3$ (BCZT) ceramic was prepared by the conventional solid-state reaction route. The detailed experimental procedure and samples' characterisations are provided in Section S1 in the ESI.†

3. Results and discussions

3.1 Structural properties

The room-temperature XRD pattern obtained for BCZT sample is displayed in Fig. 1a. The BCZT ceramic was crystallised in a pure perovskite structure without any secondary phase or impurities. The reflection peaks can be indexed according to standard $BaTiO_3$ perovskite structures with orthorhombic (O, space group: *Amm*2) (PDF #75-1608) as well as tetragonal (T, space group: *P*4*mm*). The amplified XRD fitting pattern around $2\theta \approx 45°$ using Lorentz fitting method is plotted in the inset of the Fig. 1a. This inset clearly illustrates that BCZT sample exhibits a triplet around 45° which is attributed to $(022)_O/(200)_T/$

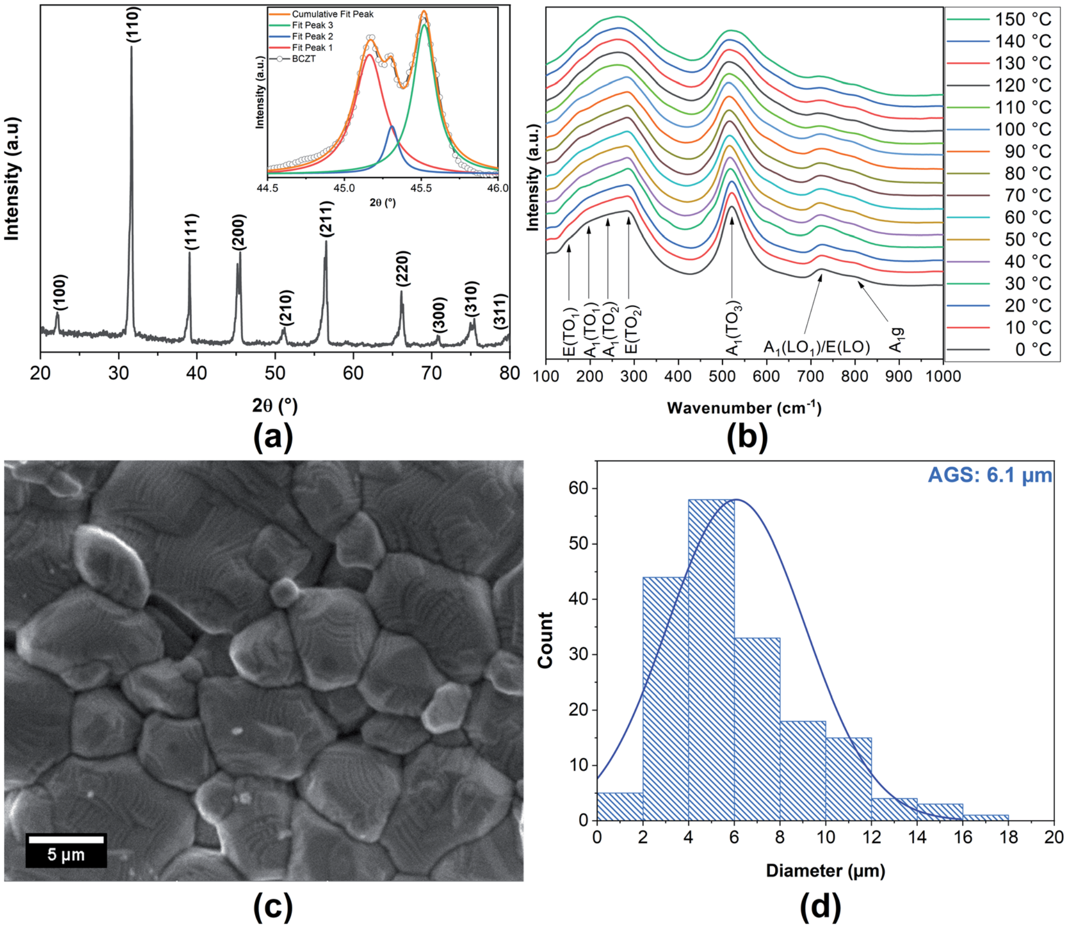

Fig. 1 (a) XRD pattern at room temperature (in the inset the enlarged peaks splitting around $2\theta \approx 45°$), (b) thermal-evolution of the Raman spectra, (c) SEM micrograph and (d) grain size distribution of BCZT ceramic.

$(200)_O$ characterising the formation of BCZT sample at the Morphotropic Phase Boundary (MPB) with the coexistence of O and T-phases.[25,26]

The dynamic properties of BCZT sample were thoroughly investigated by Raman spectroscopy within the temperature range 0–150 °C. The results of the measurements are depicted in Fig. 1b. Below room temperature, we observe the most intensive Raman peaks at frequencies of ~164, 210, 261, 294, 520, 724 and 800 cm^{-1}, which correspond to the $E(TO_1)$, $A_1(TO_1)$, $A_1(TO_2)$, $E(TO_2)$, $A_1(TO_3)$, $A_1(LO_2)/E(LO)$ and A_{1g} modes respectively. The E(TO, LO)- and A_1(TO, LO)-type modes are polar and associated with the ferroelectric phase in perovskite oxides.[27] On heating, their intensities steadily decrease, indicating the approach to the ferroelectric-to-paraelectric phase transition.[11,13,17] Above the Curie temperature, in the cubic paraelectric phase, they disappear and only two disorder-activated broad peaks centred at 260 and 514 cm^{-1} are observed. It is worth noting that the A_{1g} octahedral breathing mode at ~800 cm^{-1} persisting in the whole range of the temperatures is not related with the structural distortion of the ferroelectric phase but results instead from the local distortions, caused either by the presence of B-sites occupied by cations of different sizes (Zr^{4+}/Ti^{4+}) or from donor A-site substitutions.[13,28]

The surface morphology and the grain size (GS) distribution of BCZT ceramic examined by SEM analysis are depicted in Fig. 1c and d, respectively. It is observed that the BCZT sample exhibits a compact and dense microstructure (bulk density of 5.25 g cm^{-3}) with a non-uniform shape and dimensional grain distribution with an average grain size of 6.1 ± 3.0 μm. Also, clear grain boundaries with no porous microstructure were observed.

3.2 Dielectric properties

The thermal-evolution of the dielectric constant (ε_r) and the dielectric loss ($\tan\delta$) registered in the selected frequency window from 1 kHz to 1 MHz in the temperature range of −50 to 200 °C of BCZT ceramic are plotted in Fig. 2a. The broad anomaly corresponds to the tetragonal–cubic (T–C) phase transition around the Curie point ($T_C = 93$ °C), where ε_r and $\tan\delta$ reached 5400 and 0.019 at 1 kHz, respectively. The broad bump around room temperature was fitted using Lorentz fitting method to reveal the inherent O–T transition in BCZT ceramic[29,30] and a broad peak at 35 °C was found as depicted in the inset of Fig. 2a. In a nutshell, the detailed analysis of temperature-dependence Raman spectroscopy can provide the evidence of the O–T and T–C phase transitions.[31,32] Fig. 2b presents the thermal-evolution of the dielectric constant at 1 kHz with the peak positions of the $E(TO_2)$ Raman mode. The three apparent Raman shift plateaus correspond to the O, T and C phases, respectively, and the two drops match the O–T (<40 °C) and T–C (<100 °C) phase transitions. A typical relaxor behaviour is revealed by increasing the frequency due to the shift of the T_{O-T} and T_C peaks to the high temperatures (reminiscent of relaxor behaviour).[33] The detailed discussion of the relaxor properties of BCZT ceramic is provided in Section S2 in the ESI.† Hence, BCZT ceramic exhibits a γ value of 1.74 and a degree of deviation (ΔT_m) of the ε_r from the Curie–Weiss law above T_C of 32 °C. These values indicate a strong diffused phase transition. Hanani *et al.*[29] reported comparable values of 1.75 and 37 °C for γ and ΔT_m, respectively, for the same BCZT composition.

3.3 Ferroelectric properties

The thermal-evolution of the polarisation–electric field hysteresis loops (*P*–*E*) obtained under 25 kV cm^{-1} and at 10 Hz for BCZT ceramic are plotted in Fig. 3a. The coercive field (E_c), the remnant polarisation (P_r) and the maximum polarisation (P_{max}) obtained at room temperature are 4.65 kV cm^{-1}, 6.33 and 15.31 μC cm^{-2}, respectively. With rising the temperature, the *P*–*E* loops turn out to be slimmer, and the ferroelectric parameters decline gradually due to the disappearance of ferroelectric domains. Below the Curie temperature ($T_C = 93$ °C), the *P*–*E* curves are slim but not linear, which is the paraelectric state's characteristic. This nature can be related to the ferroelectric

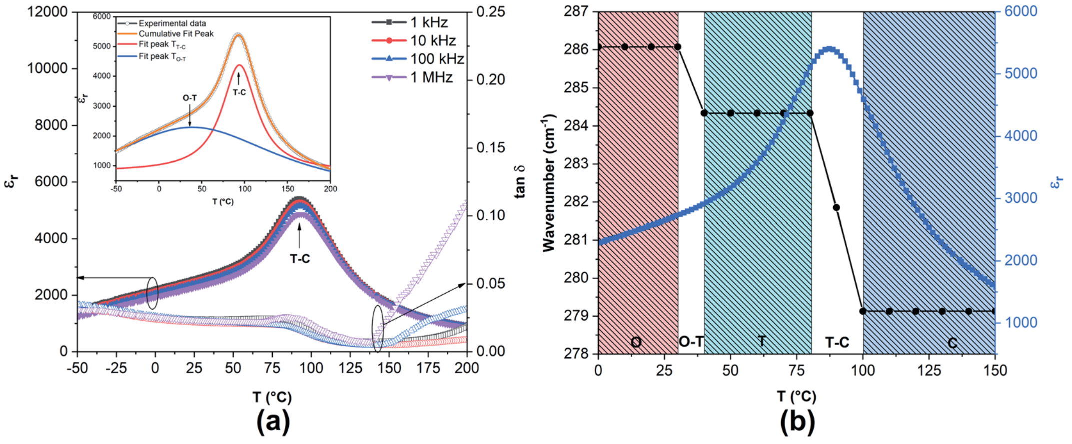

Fig. 2 Temperature-dependence of (a) ε_r and $\tan\delta$ at different frequencies (in the inset the deconvolution of the peak temperatures (T_C and T_{O-T}) of the ε_r at 1 kHz). (b) Thermal-evolution of ε_r at 1 kHz and $E(TO_2)$ mode peak position of BCZT sample.

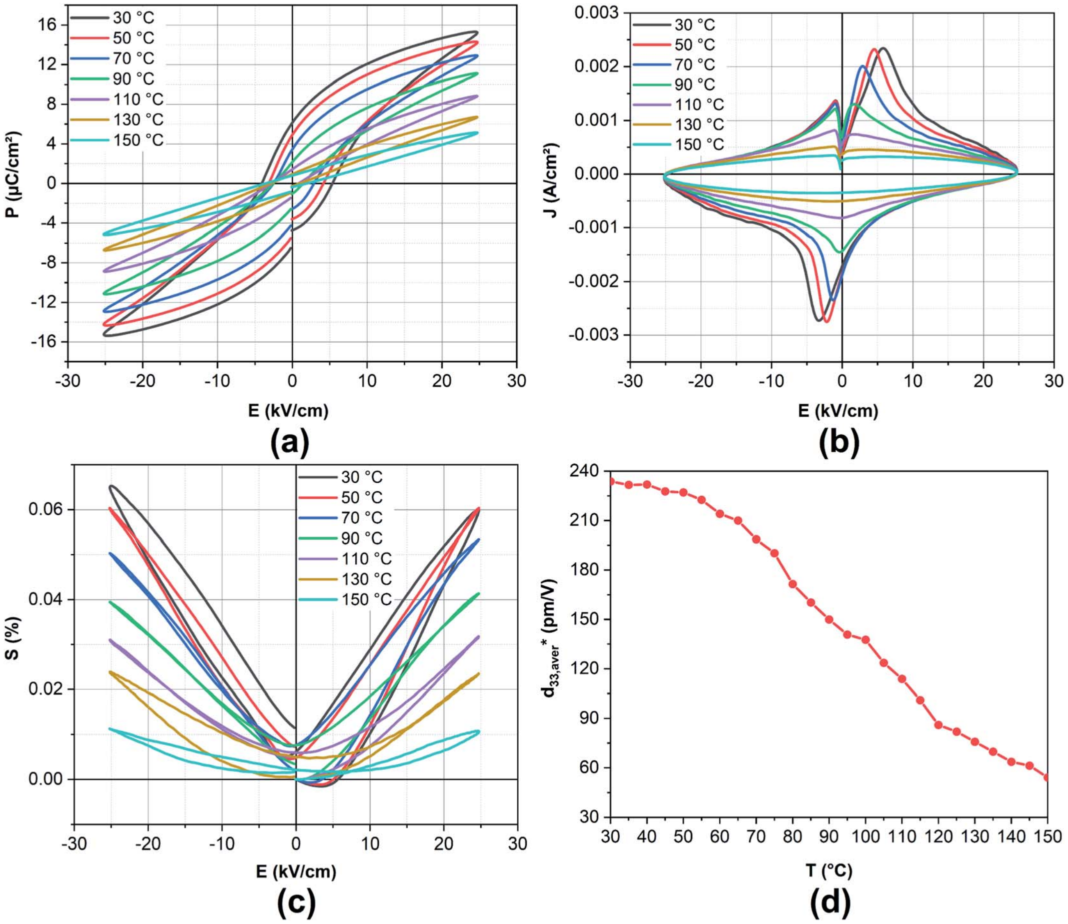

Fig. 3 Temperature-dependence of (a) P–E, (b) J–E, (c) S–E loops measured at 25 kV cm^{-1} and 10 Hz and (d) the large-signal piezoelectric coefficient (d_{33}^*) determined in BCZT ceramic.

clusters or residual polar nanoregions (PNR), which can be attributed to relaxor behaviour.[11]

Correspondingly, the temperature-dependence of the current density–electric field (J–E) curves of BCZT ceramic are displayed in Fig. 3b. It is worthy to note that when an electric field is applied to ferroelectric materials, two types of current density signals are detected, leakage current and current due to domain switching phenomena. Therefore, the electric peak appeared around the coercive field is mostly attributed to the ferroelectric domain switching.[13] Meanwhile, the E_c value obtained in the P–E and J–E curves is almost the same.[34] The domain switching current density peak around the E_c confirms the domain structure and long-range ferroelectric order of BCZT ceramic. As increasing the applied electric field to reach 25 kV cm^{-1}, the magnitude of leakage current becomes very low.[34] However, as increasing the temperature, the domain switching current peaks practically disappear, demonstrating long-range ferroelectric order disruption.[13,35]

3.4 Piezoelectric properties

The piezoelectric effect is a unique property of certain crystals that generate an electric field or a current if subjected to physical constraints and *vice versa*.[36] When an electric field is imposed on the crystal, stress on its structure is induced (indirect piezoelectric effect), this property is mostly used in actuators.[37] To evaluate the indirect piezoelectric effect's thermal-stability, the temperature-dependence of the strain–electric field (S–E) hysteresis loops of BCZT ceramic at 25 kV cm^{-1} is presented in Fig. 3c. A butterfly-like shape was observed at temperatures below T_C due to the lattice distortion and the switching and movement of domain walls by the electric field.[15,38,39] Consequently, the maximal average strain ($S_{\max}$) was found to be 0.062%. However, a sprout-like shape was noticed at higher temperatures due to the ferroelectricity's gradual disruption.[40] The corresponding large-signal piezoelectric coefficient ($d_{33}^* = S_{\max}/E_{\max}$), where, $S_{\max}$ is the maximum strain measured at the maximum electric field $E_{\max}$. The thermal-evolution of the average value of d_{33}^* ($d_{33,\mathrm{ave}}^*$) at the positive and the negative electric field is depicted in Fig. 3d. A small variation of $d_{33,\mathrm{ave}}^*$ was observed below 50 °C, nevertheless, as increasing the temperature, a gradual decrease of $d_{33,\mathrm{ave}}^*$ was detected letting a maximal $d_{33,\mathrm{ave}}^*$ value of 234 pm V^{-1} at 30 °C.

Praveen *et al.*[41] stated that BZT–52BCT ceramic exhibits a comparable strain and d_{33}^* values of 0.076% and 250 pm V^{-1}, respectively, under 30 kV cm^{-1} and at 40 °C, this value is comparable to that obtained in our BCZT ceramic. Moreover, Merselmiz *et al.*[38] reported that $Ba_{0.80}Ca_{0.20}Zr_{0.02}Ti_{0.98}O_3$ ceramic displays a maximum value of strain and d^*_{33} of 0.078% and 310 pm V^{-1}, respectively, under 25 kV cm^{-1} and at 110 °C. Besides, Chaiyo *et al.*[42] stated that $Ba_{0.80}Ca_{0.20}Zr_{0.05}Ti_{0.95}O_3$ ceramic exhibits d^*_{33} of 284 pm V^{-1} under 30 kV cm^{-1}. However, at the similar electric field, Pisitpipathsin *et al.*[43] reported high strain and d^*_{33} of 0.15% and 513 pm V^{-1}, respectively, in $Ba_{0.91}Ca_{0.09}Zr_{0.04}Ti_{0.96}O_3$ ceramic around 123 °C. Moreover, at 70 kV cm^{-1}, $Ba_{0.85}Ca_{0.15}Zr_{0.90}Ti_{0.10}O_3$ ceramic shows a similar strain (0.066%) and high d^*_{33} value of 942 pm V^{-1} at room temperature, as reported by Praveen *et al.*[44] Besides, Cai *et al.*[15] observed that as increasing the grain size (from 8.25 μm to 44.37 μm), the strain increases (0.086% to 0.115%) and correspondingly, d^*_{33} values enhanced (from 427.7 to 574.25 pm V^{-1}). It should be mentioned that the piezoelectric parameters depend strongly on the extrinsic contribution, which occurs principally from the motion of the domain walls owing to the grain size effect.[44] In other words, the domain in the coarse and large grain is easier to switch than in small grain, leading to an improved piezoelectric response.[15] Furthermore, the differences in the results could be likewise ascribed to the chemical compositions, the sintering temperature, the applied electric field, the poling effect and the measurement conditions.[45]

3.5 Energy storage performances

BCZT ferroelectric relaxor materials draw much attention for energy applications due to their excellent dielectric and ferroelectric properties.[46–48] The energy storage density can be easily obtained from the polarisation *versus* electric field (*P*–*E*) curves by integrating the area between the polarisation axis and the *P*–*E* curve.[11] As shown in Fig. 4a, the green area is equal to the recoverable energy density (W_{rec}), which corresponds to the released energy density in the discharging process. Meanwhile, the red area is equivalent to the dissipated energy density (W_{loss}) due to the dielectric material's losses. The overall area of the two parts equals the total energy density stored in the charging process. It is also required to estimate energy efficiency (η) for evaluating the energy storage performances. Thus, W_{tot} and W_{rec}, including η, could be estimated by employing eqn (1)–(3), where P, P_r, P_{max}, E, denote polarisation, remnant polarisation, maximum polarisation, and electric field, respectively.

$$W_{tot} = \int_0^{P_{max}} E\mathrm{d}P, \tag{1}$$

$$W_{rec} = \int_{P_r}^{P_{max}} E\mathrm{d}P, \tag{2}$$

$$\eta\ (\%) = \frac{W_{rec}}{W_{tot}} \times 100 = \frac{W_{rec}}{W_{rec} + W_{loss}} \times 100. \tag{3}$$

It is worth recalling that optimising the electrical breakdown strength, maximal polarisation, dielectric constant and dielectric loss of relaxor ferroelectric based-ceramics is the main

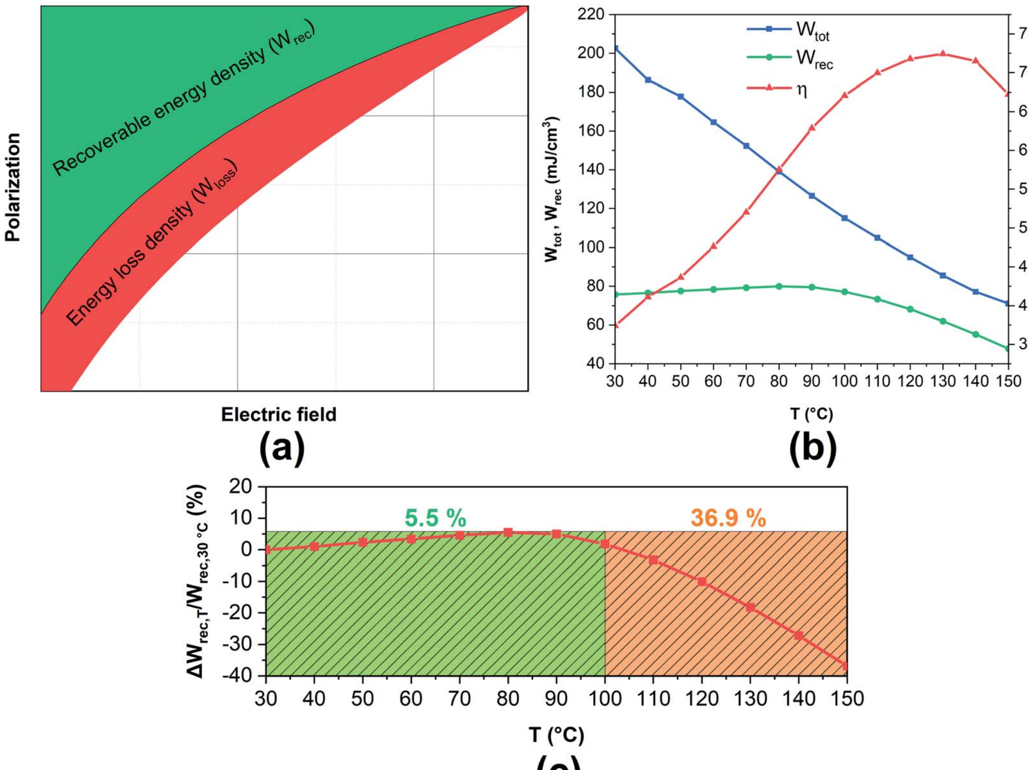

Fig. 4 (a) A schematic representation of the relevant energy storage parameters determined *via* *P*–*E* hysteresis loops. (b) Temperature-dependence of W_{tot}, W_{rec} and η. (c) Thermal-stability of the recovered energy density ($\Delta W_{rec,T}/W_{rec,30°C}$) of the BCZT ceramic at 25 kV cm^{-1}.

Table 1 Comparison of the energy storage properties of BCZT ceramic with other lead-free ceramics reported in the literature

Ceramic	W_{tot} (mJ cm^{-3})	W_{rec} (mJ cm^{-3})	η (%)	E (kV cm^{-1})	T (°C)	Ref.
BCZT	202	75	37	25	30	This work
BCZT	85	62	72.9	25	130	This work
$Ba_{0.85}Ca_{0.15}Zr_{0.90}Ti_{0.10}O_3$	136.7	97.4	71.3	20	27	11
$Ba_{0.85}Ca_{0.15}Zr_{0.90}Ti_{0.10}O_3$	113.8	38.6	33.9	20	25	15
$Ba_{0.85}Ca_{0.15}Zr_{0.90}Ti_{0.10}O_3$	90.2	71.2	78.9	20	100	15
$Ba_{0.85}Ca_{0.15}Zr_{0.90}Ti_{0.10}O_3$	526.6	414.1	78.6	60	107	11
$Ba_{0.85}Ca_{0.15}Zr_{0.90}Ti_{0.10}O_3$	480.3	280	58.3	60	RT	48
$BaTi_{0.89}Sn_{0.11}O_3$	85.1	72.4	85.07	25	30	53
$BaZr_{0.05}Ti_{0.95}O_3$	302	218	72	50	RT	54
$Bi_{0.48}La_{0.02}Na_{0.40}K_{0.10}Ti_{0.98}Zr_{0.90}Ti_{0.10}O_3$	1033	630	61	60	25	55
$0.8[0.9(Bi_{0.5}Na_{0.5})TiO_3–0.1BiScO_3]–0.2BaTiO_3$	893.65	563	63	70	RT	24
$0.525Bi_{0.5}Na_{0.5}TiO_3–0.475Ba_{0.85}Ca_{0.15}Ti_{0.9}Zr_{0.1}O_3$	990	640	62.81	77.2	RT	5
$Ba_{0.95}Ca_{0.05}Zr_{0.30}Ti_{0.70}O_3$	810.4	590	72.8	160	RT	50
$0.85(Bi_{0.47}La_{0.03}Na_{0.5})_{0.94}Ba_{0.06}TiO_3–0.15Sr(Sc_{0.5}Nb_{0.5})O_3$	2230	1830	82.32	185	RT	56

avenue to realise extremely high energy storage densities and efficiencies.[49] The thermal-evolution of the energy storage parameters of BCZT sample at 25 kV cm^{-1} is displayed in Fig. 4b. At room temperature, W_{tot}, W_{rec} and η were found to be 202, 75 mJ cm^{-3} and 37%, respectively. However, as increasing the temperature, W_{tot} declines continuously, and W_{rec} remains steady then decreases gradually above 90 °C. Correspondingly, η drops to reach 72.9% at 130 °C (W_{tot} = 85 mJ cm^{-1} and W_{rec} = 62 mJ cm^{-3}), then decreases. It should be noted that *P–E* loops were not fully saturated; thus, by further increasing the applied electric field, the energy density could be enhanced even more. However, the electric field was kept at 25 kV cm^{-1} to avoid the electric breakdown at high temperatures.

To compare the energy storage performances of BCZT sample with other lead-free ferroelectric ceramics, Table 1 summarises the W_{tot}, W_{rec} and η of bulk ceramics that have been recently reported at different applied electric fields. In the first five comparisons reported in Table 1, the energy storage performances of BCZT ceramic with the composition $Ba_{0.85}Ca_{0.15}Zr_{0.1}Ti_{0.9}O_3$ under different applied electric fields, at room temperature and the temperature corresponding to the maximal energy storage efficiency (η), are presented. For instance, at room temperature and relatively the same electric field (20 kV cm^{-1}), our sample shows enhanced results compared to those reported by Cai *et al.*[15] Meanwhile, at room temperature, Hanani *et al.*[11] stated a W_{rec} of 97.4 mJ cm^{-3} and η of 71.3% in $Ba_{0.85}Ca_{0.15}Zr_{0.1}Ti_{0.9}O_3$ ceramic under 20 kV cm^{-1}. Increasing the applied electric field to 60 kV cm^{-1} gives higher W_{rec} of 367.2 mJ cm^{-3} with η of 67.2%. However, under 60 kV cm^{-1} and at 107 °C, W_{rec} reached 414.1 mJ cm^{-3} with η of 78.6%.[11] Besides, in the same BCZT composition, Puli *et al.*[48] achieved a high W_{rec} of 280 mJ cm^{-3} and a moderate efficiency of 58.3% at room temperature and under 60 kV cm^{-1}. At room temperature, Zhan *et al.*[50] stated high W_{rec} of 590 mJ cm^{-3} and an efficiency of 72.8% under a high applied electric field of 160 kV cm^{-1} in $Ba_{0.95}Ca_{0.05}Zr_{0.30}Ti_{0.70}O_3$ ceramic.

Besides, it is necessary to investigate the thermal-stability of energy storage capabilities as a crucial factor for electric devices in practical applications.[51] For this purpose, the temperature-dependence of the energy-storage variation (ESV) was assessed by employing the eqn (4),

$$\frac{\Delta W_{rec,T}}{W_{rec,30^\circ C}} = \left| \frac{W_{rec,T} - W_{rec,30^\circ C}}{W_{rec,30^\circ C}} \right|, \tag{4}$$

Here $W_{rec,T}$ is the W_{rec} value at a given temperature, and $\Delta W_{rec,T}$ is the difference of $W_{rec,T}$ and $W_{rec,30^\circ C}$.

The thermal-evolution of the ESV values in BCZT ceramic is plotted in Fig. 4c. It can be seen that the ESV value of BCZT ceramic process excellent stability less than ±5.5% (W_{rec} = 75.8–77.2 mJ cm^{-3}) in the temperature range of 30–100 °C. Nevertheless, above 100 °C, the ESV value reached 36.9% due to the ferroelectric–paraelectric phase transition. The obtained results are very promising in comparison to other ferroelectric materials. Xu *et al.*[51] reported that the ESV value of BCZT-0.5 wt% MgO ceramic was ±14.18% despite the high recoverable energy storage W_{rec} of 93.2 mJ cm^{-3} in a broad temperature range of 20–120 °C under 35 kV cm^{-1}. Besides, Hanani *et al.*[11] claimed a remarkable ESV value (fluctuation less than ±12.7%) over a temperature range of 27–127 °C under 60 kV cm^{-1}. Besides, Jayakrishnan *et al.*[52] reported that $0.6BaZr_{0.20}Ti_{0.80}O_3$–$0.4Ba_{0.70}Ca_{0.30}TiO_3$ ceramic exhibits a high variation rate of 46.3%, where W_{rec} dropped from 121 to 65 mJ cm^{-3} at 30 °C and 90 °C, respectively, under 25 kV cm^{-1}. Hence, BCZT ceramic presents an excellent thermal-stability over a wide temperature range related to the strengthened diffuse phase transition (DPT) behaviour of BCZT ceramic.

3.6 Electrocaloric effect

In order to assess the capabilities of BCZT ceramic for eco-friendly solid-state cooling devices, the ECE was investigated by the indirect measurements based on the recorded ferroelectric order parameter P (E, T) determined from the *P–E* hysteresis loops (see Fig. 3a). At every fixed applied electric field, a fifth-order polynomial fitting of the upper polarisation branches was performed.[16] Then, the evolution of the polarisation as a function of the temperature was deduced (see

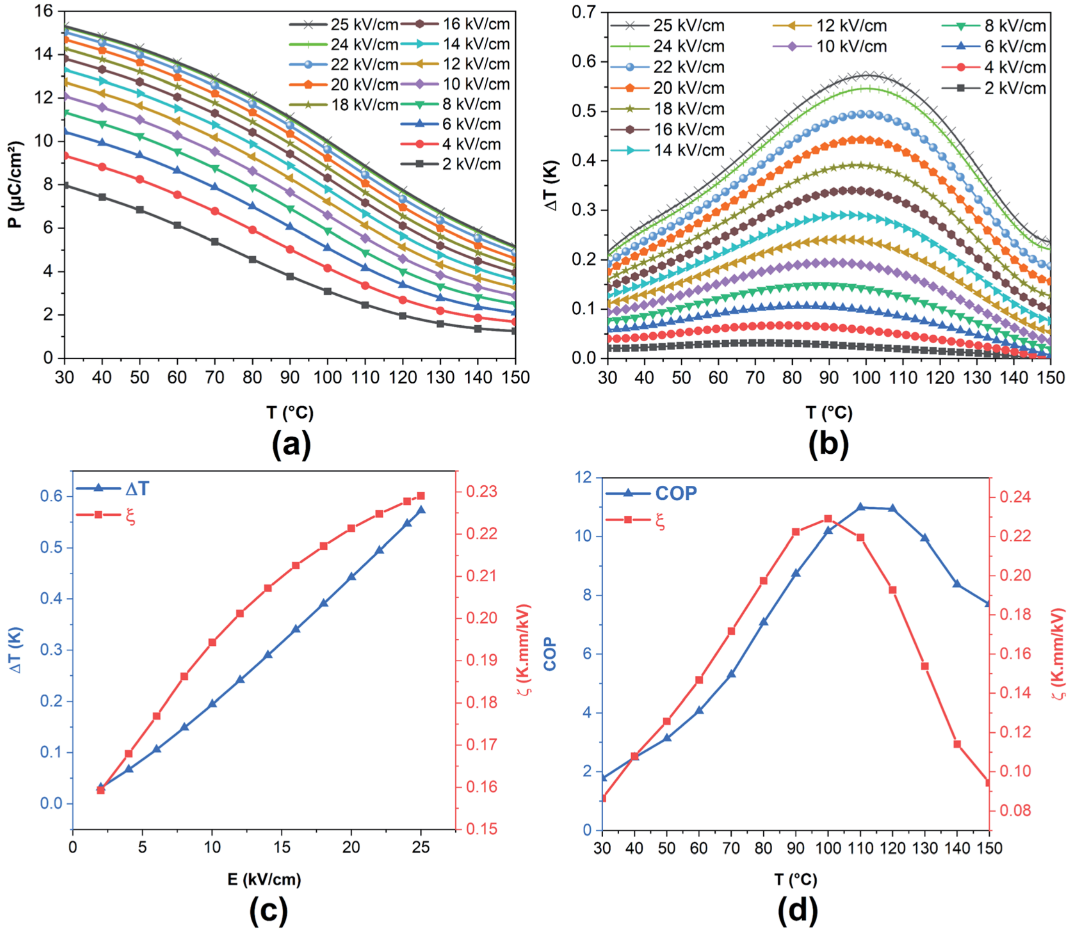

Fig. 5 Thermal-evolution of (a) P and (b) ΔT at different applied electric fields. Electric field-dependence of (c) ΔT and ζ near the T_C. (d) Thermal-evolution of COP and ζ in BCZT ceramic under 25 kV cm^{-1}.

Fig. 5a). Obviously, with increasing the temperature, the polarisation declines gradually then drops at higher temperatures. The isothermal entropy change (ΔS) and the electrocaloric temperature change (ΔT) were estimated by employing the Maxwell relation (eqn (5) and (6)), where, ρ and C_P denote the mass density and the specific heat of the sample, respectively. The value of C_P was obtained from ref. 20.

$$\Delta S = \int_{E_1}^{E_2} \left(\frac{\partial P}{\partial T}\right)_E \mathrm{d}E, \tag{5}$$

$$\Delta T = -\int_{E_1}^{E_2} \frac{T}{\rho C_P} \left(\frac{\partial P}{\partial T}\right)_E \mathrm{d}E. \tag{6}$$

Fig. 5b displays the temperature-dependence of the reversible electrocaloric temperature change (ΔT) under several applied electric fields in BCZT ceramic. The maximum of ECE is closely related to the ferroelectric–paraelectric phase transition resulting in a broad ECE peak exhibiting a maximum around T_C. As increasing the applied electric fields, ΔT increases and its maximum shifts toward higher temperatures, indicating that T_C shifts up to higher temperatures. At 25 kV cm^{-1}, ΔT achieves a maximum of 0.57 K locates at T = 100 °C and the corresponding ΔS was found to be 0.61 J kg^{-1} K^{-1}. Afterwards, ΔT diminishes gradually with increasing the temperature, owing to the disruption of the polarisation (*i.e.*, the extracted polarization gradient $(\partial P/\partial T)_E$ above T_C). This finding is in accordance with the dielectric properties data. Fig. 5c shows the plots of ΔT *versus* the applied electric fields, and the corresponding EC responsivity defined as $\zeta = \Delta T/\Delta E$ at the peak temperature. ΔT increases with increasing the applied electric field; in contrast, ζ increases rapidly at low electric fields, then starts to saturate to reach a maximum of 0.23 K mm kV^{-1} at 25 kV cm^{-1}.

Table 2 compares the EC response of BCZT ceramic with other lead-free ceramics. At 14 kV cm^{-1}, Merselmiz *et al.*[38] reported that $Ba_{0.80}Ca_{0.15}Zr_{0.02}Ti_{0.98}O_3$ sample exhibits high ΔT and ζ of 0.668 K and 0.477 around T_C = 112 °C under 14 kV cm^{-1} determined by the direct method. Moreover, a comparable result of ΔT = 0.565 K and ζ = 0.188 K mm kV^{-1} was found in $Ba_{0.30}Ca_{0.10}Zr_{0.05}Ti_{0.95}O_3$ ceramic around T_C = 119 °C as reported by Ben Abdessalem *et al.*[22] At 60 kV cm^{-1}, Hanani *et al.*[11] stated high ΔT = 1.479 K and ζ = 0.246 K mm kV^{-1} around T_C = 94 °C in $Ba_{0.85}Ca_{0.15}Zr_{0.10}Ti_{0.90}O_3$ ceramic. Wang *et al.*[57] reported comparable ΔT of 0.6 K in

Table 2 Comparison of the EC response of BCZT sample with other lead-free ceramics reported in the literature

Ceramic	T (°C)	ΔT (K)	ΔE (kV cm^{-1})	ζ (K mm kV^{-1})	Ref.
BCZT	100	0.57	25	0.23	This work
$Ba_{0.85}Ca_{0.15}Zr_{0.10}Ti_{0.90}O_3$	100	0.152	8	0.19	19
$Ba_{0.85}Ca_{0.15}Zr_{0.10}Ti_{0.90}O_3$	74	0.155	8	0.194	11
$Ba_{0.85}Ca_{0.15}Zr_{0.10}Ti_{0.90}O_3$	82	0.459	20	0.229	11
$Ba_{0.85}Ca_{0.15}Zr_{0.10}Ti_{0.90}O_3$	87	0.492	17	0.289	16
$Ba_{0.85}Ca_{0.15}Zr_{0.10}Ti_{0.90}O_3$	97	0.4	21.5	0.186	73
$Ba_{0.85}Ca_{0.15}Zr_{0.10}Ti_{0.90}O_3$	94	1.479	60	0.246	11
$Ba_{0.80}Ca_{0.15}Zr_{0.02}Ti_{0.98}O_3$	112	0.668	14	0.477	38
$Ba_{0.80}Ca_{0.20}Zr_{0.02}Ti_{0.98}O_3$	112	0.68	24	0.283	38
$Ba_{0.30}Ca_{0.10}Zr_{0.05}Ti_{0.95}O_3$	119	0.565	30	0.188	22
$Ba_{0.98}Ca_{0.02}Zr_{0.085}Ti_{0.915}O_3$	85	0.6	40	0.15	57
BZT–30BCT	60	0.30	20	0.15	74
BZT–32BCT	64	0.33	20	0.165	75
$BaTi_{0.89}Sn_{0.11}O_3$	52	0.71	25	0.284	53

$Ba_{0.98}Ca_{0.02}Zr_{0.085}Ti_{0.915}O_3$ ceramic but under a higher electric field of 40 kV cm^{-1}.

Moreover, Fig. 5d depicts the thermal-evolution of ζ at 25 kV cm^{-1}, showing a broad peak around 100 °C. It should be mentioned that the electrocaloric effects preserve significant values over a broad temperature span (T_{span}). This temperature span represents a crucial parameter for practical cooling applications in which a large ECE can be maintained and is usually given as the full width at half maximum (FWHM) of the ECE peak. It was reported that the diffuse phase transition is directly related to broadened EC peaks under the low electric field.[58] The obtained T_{span} value is 70 K, which indicates that a large ECE can be maintained over a broad temperature range of 70 K. This can be explained by the diffuse phase transition contribution ($\gamma = 1.74$) in diffuse ferroelectrics, where the PNRs are very sensitive to frequency and magnitude of external electric field and can occur in a broad temperature range around T_C.[59]

Another essential parameter to evaluate the ECE materials' ability for application in the solid-state cooling devices is the refrigerant capacity RC = $\Delta S T_{\text{span}}$.[11,60] The obtained value of RC was found to be 42.7 J kg^{-1} at 25 kV cm^{-1}. The coefficient of performance (COP) is considered an essential parameter to estimate the cooling cycle performance and assess the material's efficiency.[61,62] The COP is estimated by the eqn (7),[61] where Q refers to the isothermal heat,

$$\text{COP} = \frac{|Q|}{|W_{\text{tot}}|} = \frac{|T\Delta S|}{|W_{\text{tot}}|}. \tag{7}$$

Fig. 5d illustrates the thermal-evolution of the COP from 30 to 150 °C in BCZT ceramic under 25 kV cm^{-1}. The COP is evidenced by a broad peak in the whole temperature range, with a maximum value of 11 at 110 °C, then slightly decreases. The obtained value is comparable to some previous works of Pb-free[63–67] and Pb-based[61,68–72] materials. For example, Kumar *et al.*[65] presented that $0.97K_{0.5}Na_{0.5}NbO_3$–$0.03LiSbO_3$ nanocrystalline ceramic demonstrated a COP value of 8.14 under an electric field of 40 kV cm^{-1}. Peng *et al.*[70] obtained a COP value of 3.37 in Nb-doped $Pb_{0.99}(Zr_{0.65}Sn_{0.3}Ti_{0.05})_{0.98}O_3$ antiferroelectric thin film by using a sol–gel route. In addition, Hanani *et al.*[11] stated a COP value of 6.29 at 92 °C under 55 kV cm^{-1} in $Ba_{0.85}Ca_{0.15}Zr_{0.10}Ti_{0.90}O_3$ ceramic prepared by hydrothermal method. We conclude that BCZT ceramic is a favourable material for ECE cooling system applications, owing to its enhanced values of ΔT, ζ, T_{span}, RC and COP at a moderate applied electric field.

4. Conclusions

The structure, electric, piezoelectric, energy storage and electrocaloric properties of lead-free BCZT ceramic prepared by solid-state reaction route were investigated. The phase transitions in BCZT ceramic were demonstrated through Raman spectroscopy's temperature-dependence, dielectric and ferroelectric measurements. Besides, enhanced piezoelectric properties ($d_{33}^* = 234$ pm V^{-1} at 30 °C) and energy storage performances ($W_{\text{rec}} = 62$ mJ cm^{-3} and $\eta = 72.9\%$ at 130 °C) were obtained. The recovered energy density's thermal-stability shows an excellent ESV value less than ±5.5% in the temperature range of 30–100 °C, at 25 kV cm^{-1}. Furthermore, enhanced electrocaloric values of $\Delta T = 0.57$ K, $\Delta S = 0.61$ J kg^{-1} K^{-1}, $\zeta = 0.23$ K mm kV^{-1}, $T_{\text{span}} = 70$ °C, RC = 42.7 J kg^{-1} and COP = 11 in BCZT ceramic were determined by using the Maxwell relation as an indirect method. Hence, the eco-friendly BCZT ceramic results are enhanced and make it a potential candidate for energy storage density capacitors and solid-state electrocaloric cooling technologies.

Conflicts of interest

There are no conflicts to declare.

Acknowledgements

The authors gratefully acknowledge the generous financial support of CNRST Priority Program PPR 15/2015, and the European Union Horizon 2020 Research and Innovation actions

MSCA-RISE-ENGIMA (No. 778072) and MSCA-RISE-MELON (No. 872631). Z. K. and B. R. acknowledge Slovenian Research Agency grant J1-9147 and program P1-0125.

References

1 P. K. Panda and B. Sahoo, *Ferroelectrics*, 2015, **474**, 128–143.

2 T. R. Shrout and S. J. Zhang, *J. Electroceram.*, 2007, **19**, 111–124.

3 J. Koruza, A. J. Bell, T. Frömling, K. G. Webber, K. Wang and J. Rödel, *J. Mater.*, 2018, **4**, 13–26.

4 Z. Hanani, I. Izanzar, M. Amjoud, D. Mezzane, M. Lahcini, H. Uršič, U. Prah, I. Saadoune, M. El Marssi, I. A. Luk'yanchuk, Z. Kutnjak and M. Gouné, *Nano Energy*, 2021, **81**, 105661.

5 M. Yao, Y. Pu, L. Zhang and M. Chen, *Mater. Lett.*, 2016, **174**, 110–113.

6 E. Cross, *Nature*, 2004, **432**, 24–25.

7 W. Liu and X. Ren, *Phys. Rev. Lett.*, 2009, **103**, 257602.

8 X. Liu, Z. Chen, B. Fang, J. Ding, X. Zhao, H. Xu and H. Luo, *J. Alloys Compd.*, 2015, **640**, 128–133.

9 H. Bao, C. Zhou, D. Xue, J. Gao and X. Ren, *J. Phys. D: Appl. Phys.*, 2010, **43**, 465401.

10 J. Wu, in *Advances in Lead-Free Piezoelectric Materials*, Springer Singapore, Singapore, 2018, pp. 247–299.

11 Z. Hanani, S. Merselmiz, D. Mezzane, M. Amjoud, A. Bradeško, B. Rožič, M. Lahcini, M. El Marssi, A. V. Ragulya, I. A. Luk'Yanchuk, Z. Kutnjak and M. Gouné, *RSC Adv.*, 2020, **10**, 30746–30755.

12 X. Q. Liu, T. T. Chen, M. Sen Fu, Y. J. Wu and X. M. Chen, *Ceram. Int.*, 2014, **40**, 11269–11276.

13 Z. Hanani, D. Mezzane, M. Amjoud, A. G. G. Razumnaya, S. Fourcade, Y. Gagou, K. Hoummada, M. El Marssi and M. Gouné, *J. Mater. Sci.: Mater. Electron.*, 2019, **30**, 6430–6438.

14 V. S. Puli, D. K. Pradhan, D. B. Chrisey, M. Tomozawa, G. L. Sharma, J. F. Scott and R. S. Katiyar, *J. Mater. Sci.*, 2013, **48**, 2151–2157.

15 W. Cai, Q. Zhang, C. Zhou, R. Gao, S. Zhang, Z. Li, R. Xu, G. Chen, X. Deng, Z. Wang and C. Fu, *J. Mater. Sci.: Mater. Electron.*, 2020, **31**, 9167–9175.

16 Z. Hanani, S. Merselmiz, A. Danine, N. Stein, D. Mezzane, M. Amjoud, M. Lahcini, Y. Gagou, M. Spreitzer, D. Vengust, Z. Kutnjak, M. El Marssi, I. A. Luk'yanchuk and M. Gouné, *J. Adv. Ceram.*, 2020, **9**, 210–219.

17 J. Shi, R. Zhu, X. Liu, B. Fang, N. Yuan, J. Ding and H. Luo, *Materials*, 2017, **10**, 1093.

18 Y. Zhou, Q. Lin, W. Liu and D. Wang, *RSC Adv.*, 2016, **6**, 14084–14089.

19 H. Kaddoussi, A. Lahmar, Y. Gagou, B. Manoun, J. N. Chotard, J. L. Dellis, Z. Kutnjak, H. Khemakhem, B. Elouadi and M. El Marssi, *J. Alloys Compd.*, 2017, **713**, 164–179.

20 H. Kaddoussi, A. Lahmar, Y. Gagou, B. Asbani, J. L. Dellis, G. Cordoyiannis, B. Allouche, H. Khemakhem, Z. Kutnjak and M. El Marssi, *J. Alloys Compd.*, 2016, **667**, 198–203.

21 F. Weyland, R. Hayati and N. Novak, *Ceram. Int.*, 2019, **45**, 11408–11412.

22 M. Ben Abdessalem, I. Kriaa, A. Aydi and N. Abdelmoula, *Ceram. Int.*, 2018, **44**, 13595–13601.

23 Z. Kutnjak, B. Rožič and R. Pirc, in *Wiley Encyclopedia of Electrical and Electronics Engineering*, John Wiley & Sons, Inc., Hoboken, NJ, USA, 2015, pp. 1–19.

24 Y. Sun, H. Wang, G. Liu, H. Xie, C. Zhou, G. Chen, C. Yuan and J. Xu, *J. Mater. Sci.: Mater. Electron.*, 2020, **31**, 5546–5553.

25 W. Cai, Q. Zhang, C. Zhou, R. Gao, F. Wang, G. Chen, X. Deng, Z. Wang, N. Deng, L. Cheng and C. Fu, *J. Mater. Sci.*, 2020, **55**, 9972–9992.

26 Z. Hanani, E. H. Ablouh, M. 'Barek Amjoud, D. Mezzane, S. Fourcade and M. Gouné, *Ceram. Int.*, 2018, **44**, 10997–11000.

27 D. A. Tenne, X. X. Xi, Y. L. Li, L. Q. Chen, A. Soukiassian, M. H. Zhu, A. R. James, J. Lettieri, D. G. Schlom, W. Tian and X. Q. Pan, *Phys. Rev. B: Condens. Matter Mater. Phys.*, 2004, **69**, 174101.

28 A. Hamza, F. Benabdallah, I. Kallel, L. Seveyrat, L. Lebrun and H. Khemakhem, *J. Alloys Compd.*, 2018, **735**, 2523–2531.

29 Z. Hanani, D. Mezzane, M. Amjoud, S. Fourcade, A. G. G. Razumnaya, I. A. A. Luk'yanchuk and M. Gouné, *Superlattices Microstruct.*, 2019, **127**, 109–117.

30 M. Acosta, N. Novak, W. Jo and J. Rödel, *Acta Mater.*, 2014, **80**, 48–55.

31 C. Zhao, H. Wu, F. Li, Y. Cai, Y. Zhang, D. Song, J. Wu, X. Lyu, J. Yin, D. Xiao, J. Zhu and S. J. Pennycook, *J. Am. Chem. Soc.*, 2018, **140**, 15252–15260.

32 M. H. Zhang, K. Wang, J. S. Zhou, J. J. Zhou, X. Chu, X. Lv, J. Wu and J. F. Li, *Acta Mater.*, 2017, **122**, 344–351.

33 A. A. Bokov and Z. G. Ye, in *Frontiers of Ferroelectricity: A Special Issue of the Journal of Materials Science*, Springer US, Boston, MA, 2007, pp. 31–52.

34 A. Kumar, V. V. Bhanu Prasad, K. C. James Raju and A. R. James, *Eur. Phys. J. B*, 2015, **88**, 287.

35 K. Li, X. L. Zhu, X. Q. Liu and X. M. Chen, *Appl. Phys. Lett.*, 2013, **102**, 112912.

36 P. Muralt, in *Encyclopedia of Materials: Science and Technology*, Elsevier, 2001, pp. 8894–8897.

37 J. Rödel, K. G. Webber, R. Dittmer, W. Jo, M. Kimura and D. Damjanovic, *J. Eur. Ceram. Soc.*, 2015, **35**, 1659–1681.

38 S. Merselmiz, Z. Hanani, S. Ben Moumen, A. Matavž, D. Mezzane, N. Novak, Z. Abkhar, L. Hajji, M. Amjoud, Y. Gagou, K. Hoummada, D. Črešnar, Z. Kutnjak and B. Rožič, *J. Mater. Sci.: Mater. Electron.*, 2020, **31**, 17018–17028.

39 U. Obilor, C. Pascual-Gonzalez, S. Murakami, I. M. Reaney and A. Feteira, *Mater. Res. Bull.*, 2018, **97**, 385–392.

40 L. Wang, W. Bai, X. Zhao, F. Wen, L. Li, W. Wu, P. Zheng and J. Zhai, *J. Mater. Sci.: Mater. Electron.*, 2019, **30**, 9219–9230.

41 J. P. Praveen, T. Karthik, A. R. James, E. Chandrakala, S. Asthana and D. Das, *J. Eur. Ceram. Soc.*, 2015, **35**, 1785–1798.

42 N. Chaiyo, D. P. Cann and N. Vittayakorn, *J. Mater. Sci.*, 2015, **50**, 6171–6179.

43 N. Pisitpipathsin, P. Kantha, K. Pengpat and G. Rujijanagul, in *Ceramics International*, Elsevier, 2013, vol. 39, pp. S35–S39.

44 J. P. Praveen, K. Kumar, A. R. James, T. Karthik, S. Asthana and D. Das, *Curr. Appl. Phys.*, 2014, **14**, 396–402.

45 Y. Zhang, H. Sun and W. Chen, *J. Phys. Chem. Solids*, 2018, **114**, 207–219.

46 X. Chen, X. Chao and Z. Yang, *Mater. Res. Bull.*, 2019, **111**, 259–266.

47 Z. Hanani, D. Mezzane, M. Amjoud, Y. Gagou, K. Hoummada, C. Perrin, A. G. Razumnaya, Z. Kutnjak, A. Bouzina, M. El Marssi, M. Gouné and B. Rožič, *J. Mater. Sci.: Mater. Electron.*, 2020, **31**, 10096–10104.

48 V. S. Puli, D. K. Pradhan, I. Coondoo, N. Panwar, S. Adireddy, S. Luo, R. S. Katiyar and D. B. Chrisey, *J. Phys. D: Appl. Phys.*, 2019, **52**, 255304.

49 L. Yang, X. Kong, F. Li, H. Hao, Z. Cheng, H. Liu, J. F. Li and S. Zhang, *Prog. Mater. Sci.*, 2019, **102**, 72–108.

50 D. Zhan, Q. Xu, D. P. Huang, H. X. Liu, W. Chen and F. Zhang, *J. Alloys Compd.*, 2016, **682**, 594–600.

51 K. Xu, P. Yang, W. Peng and L. Li, *J. Alloys Compd.*, 2020, **829**, 154516.

52 A. R. Jayakrishnan, K. V. Alex, A. Thomas, J. P. B. Silva, K. Kamakshi, N. Dabra, K. C. Sekhar, J. Agostinho Moreira and M. J. M. Gomes, *Ceram. Int.*, 2019, **45**, 5808–5818.

53 S. Merselmiz, Z. Hanani, D. Mezzane, M. Spreitzer, A. Bradeško, D. Fabijan, D. Vengust, M. Amjoud, L. Hajji, Z. Abkhar, A. G. Razumnaya, B. Rožič, I. A. Luk'yanchuk and Z. Kutnjak, *Ceram. Int.*, 2020, **46**, 23867–23876.

54 T. Badapanda, S. Chaterjee, A. Mishra, R. Ranjan and S. Anwar, *Phys. B*, 2017, **521**, 264–269.

55 P. Butnoi, S. Manotham, P. Jaita, C. Randorn and G. Rujijanagul, *J. Eur. Ceram. Soc.*, 2018, **38**, 3822–3832.

56 J. Xie, Z. Dai, X. Ding, X. Fan, W. Liu, L. Zhang and J. Li, *J. Mater. Sci.*, 2020, **55**, 13578–13589.

57 J. Wang, T. Yang, S. Chen, G. Li, Q. Zhang and X. Yao, *J. Alloys Compd.*, 2013, **550**, 561–563.

58 X. Zhang, L. Wu, S. Gao, J. Q. Liu, B. Xu, Y. D. Xia, J. Yin and Z. G. Liu, *AIP Adv.*, 2015, **5**, 047134.

59 Y. Zhao, X. Q. Liu, S. Y. Wu and X. M. Chen, *J. Electroceram.*, 2019, **43**, 106–116.

60 S. G. Lu and Q. Zhang, *Adv. Mater.*, 2009, **21**, 1983–1987.

61 Y. Zhao, X. Hao and Q. Zhang, *Ceram. Int.*, 2016, **42**, 1679–1687.

62 J. Shi, D. Han, Z. Li, L. Yang, S. G. Lu, Z. Zhong, J. Chen, Q. M. Zhang and X. Qian, *Joule*, 2019, **3**, 1200–1225.

63 R. Kumar and S. Singh, *J. Alloys Compd.*, 2018, **764**, 289–294.

64 B. Peng, Q. Zhang, B. Gang, G. J. T. Leighton, C. Shaw, S. J. Milne, B. Zou, W. Sun, H. Huang and Z. Wang, *Energy Environ. Sci.*, 2019, **12**, 1708–1717.

65 R. Kumar and S. Singh, *Sci. Rep.*, 2018, **8**, 3186.

66 R. Kumar, A. Kumar and S. Singh, *Sustainable Energy Fuels*, 2018, **2**, 2698–2704.

67 R. Kumar, D. Khurana, A. Kumar and S. Singh, *Ceram. Int.*, 2018, **44**, 20845–20850.

68 E. Defay, S. Crossley, S. Kar-Narayan, X. Moya and N. D. Mathur, *Adv. Mater.*, 2013, **25**, 3337–3342.

69 H. Gao, X. Hao, Q. Zhang, S. An and L. B. Kong, *J. Mater. Sci.: Mater. Electron.*, 2016, **27**, 10309–10319.

70 B. Peng, M. Zhang, S. Tang, J. Jiang, W. Zhao, B. Zou, N. Luo, Q. Zhang, G. J. T. Leighton, C. Shaw, L. Liu and W. Sun, *Ceram. Int.*, 2020, **46**, 4300–4306.

71 Y. Zhao, X. Hao and Q. Zhang, *ACS Appl. Mater. Interfaces*, 2014, **6**, 11633–11639.

72 X. Hao, Y. Zhao and Q. Zhang, *J. Phys. Chem. C*, 2015, **119**, 18877–18885.

73 S. Patel, P. Sharma and R. Vaish, *Phase Transitions*, 2016, **89**, 1062–1073.

74 Y. Bai, X. Han and L. Qiao, *Appl. Phys. Lett.*, 2013, **102**, 1–5.

75 M. Sanlialp, V. V. Shvartsman, M. Acosta and D. C. Lupascu, *J. Am. Ceram. Soc.*, 2016, **99**, 4022–4030.